Delft University of Technology

FUNDAMENTALS OF AEROACOUSTICS

AE4260A

Assignment: Airfoil self-noise computations and assessment of analytical models

Authors:
Austin Ramanna (4663314), Anastasios Panagiotopoulos (5350522), Mustafa Sabri Güverte (4548361)

January 19, 2022

1 Analytical model

1.1 Xfoil Implementation

To begin with, the design and analysis of the NACA 0018 airfoil were performed by the usage of X-Foil. Moreover, the limitations imposed by case 1 makes the transition feasible only by using trip strips at the airfoil surface. The layer strips are positioned at 20% of the local chord on the upper and the lower side of the airfoil. In order to compute the viscous part of the analysis, Reynolds and Mach numbers are essential. These values are assessed by case 1 and are shown in the following Equation 1 and Equation 2:

$$R_e = 273.847 \tag{1}$$

$$M_a = 0,058773 \tag{2}$$

1.1.1 Pressure distribution

To begin with, by introducing the flow condition (Table 1) for case 1 in the xfoil program, the pressure coefficient and the pressure vectors over the NACA 0018 airfoil can be derived as follows:

Table 1: Available data-set of case 1

Case 1	
Angle of attack	0°
Free-stream velocity	20 m/s

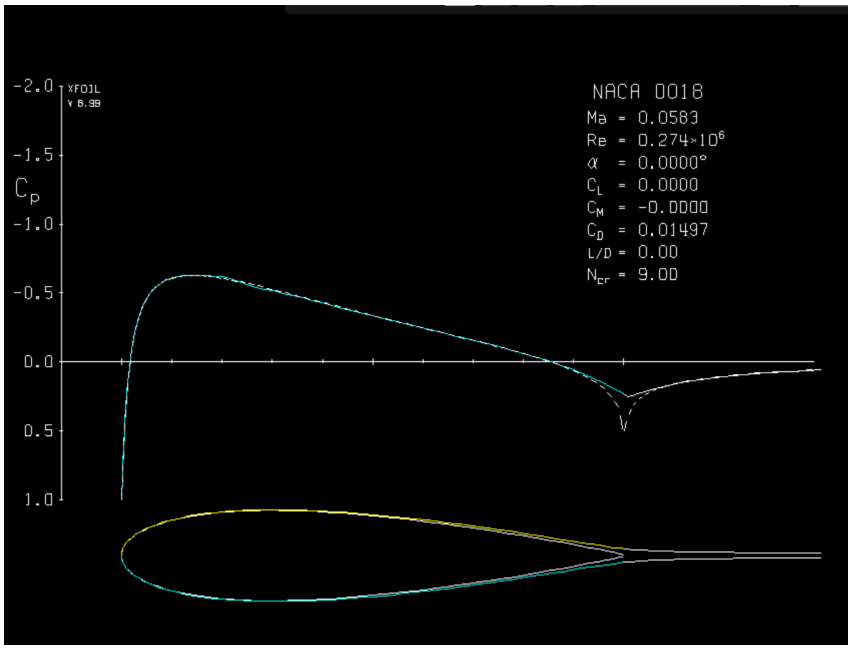

Figure 1: Pressure coefficient over the NACA0018 airfoil obtained from X-Foil

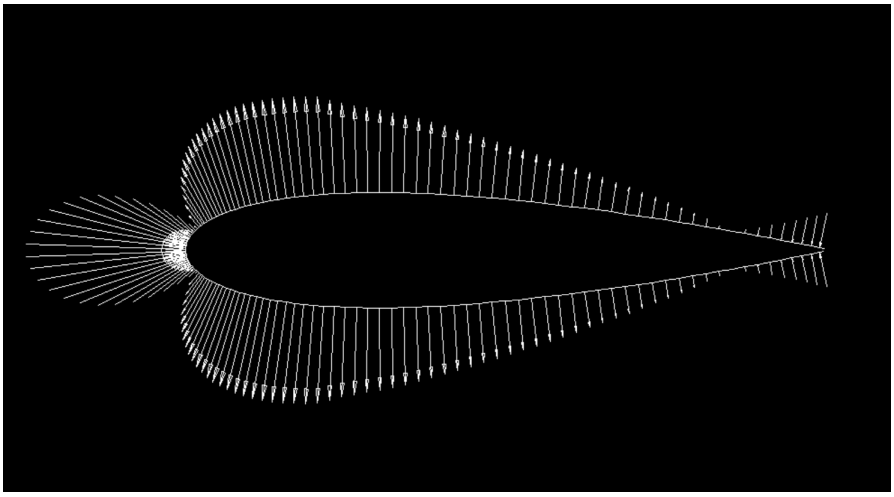

Figure 2: Pressure vectors over the NACA0018 airfoil obtained from X-Foil

The results for the pressure distribution which are demonstrated in the Figure 1 and Figure 2 are expected for a symmetric airfoil at zero angle of attack. The pressure coefficient over the upper and the lower surface of the airfoil are exactly the same. Moreover, the pressure gets maximum value at the leading edge, where velocity is null. Finally, the lift coefficient is zero and the drag coefficient becomes the minimum value, as expected for the symmetric airfoil at zero angle of attack.

To end up with, We can easily derive direct from the X-Foil the skin friction coefficient C_f and illustrate it in Figure 3:

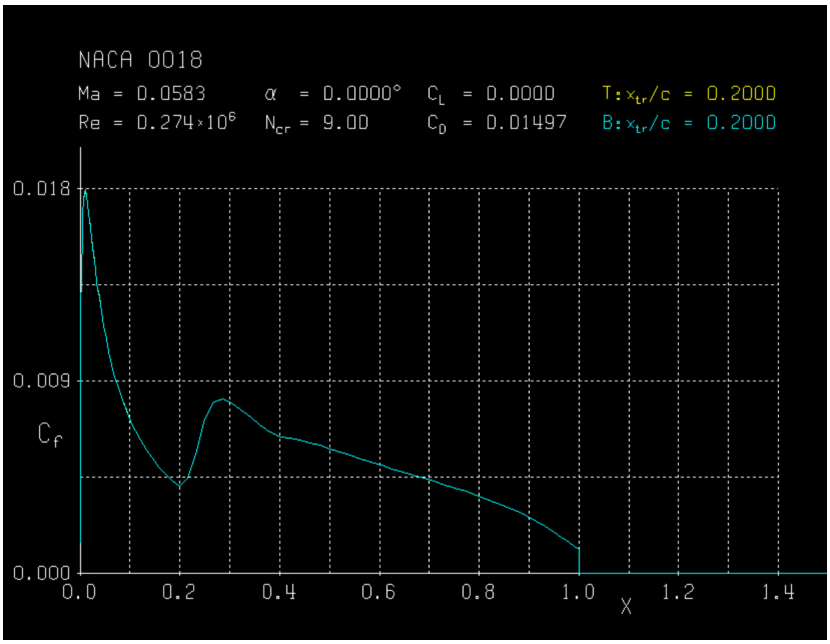

Figure 3: Skin friction coefficient of airfoil obtained from X-Foil

One can observe that the skin friction drag is the highest at the stagnation point, due to the orthogonal flow speed to the surface of the airfoil. Furthermore, the same phenomena causes a local maxima at the position of the trip strips which too cause an apposing boundary to the flow.

1.1.2 Boundary layer properties

For the calculation of the right boundary layer properties, the transition is forced at 20% of the chord as it was mentioned before. Hence, we can easily derive for the X-Foil values for the boundary layer edge velocity, displacement thickness and momentum thickness over the airfoil, as it illustrated in Figure 4 and Figure 5:

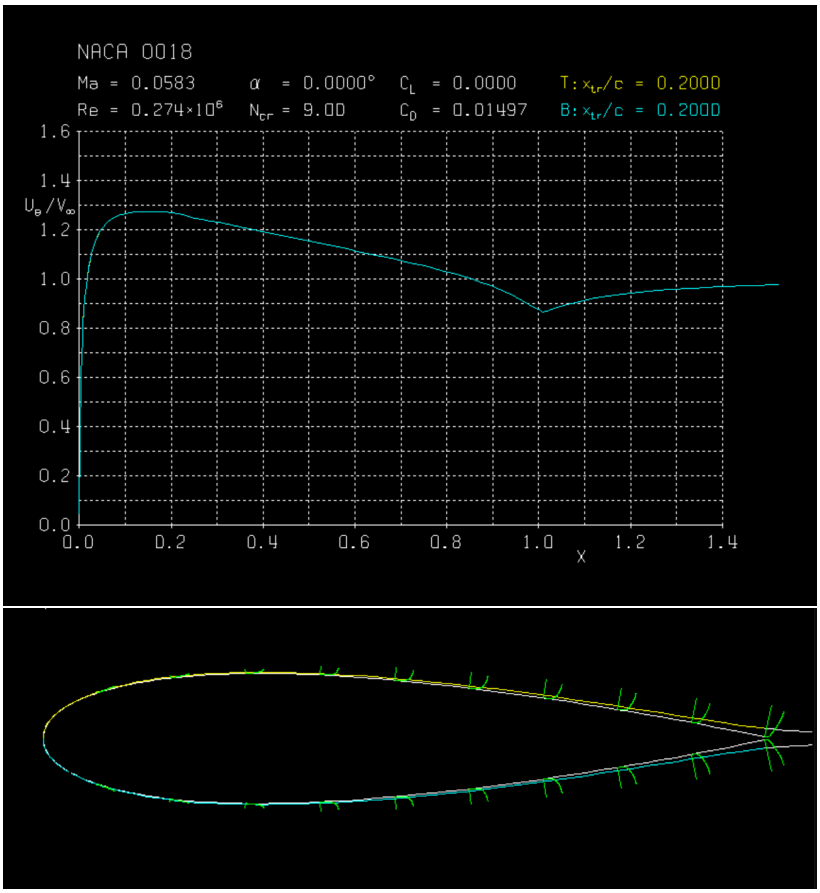

Figure 4: Boundary layer edge velocity obtained from X-Foil

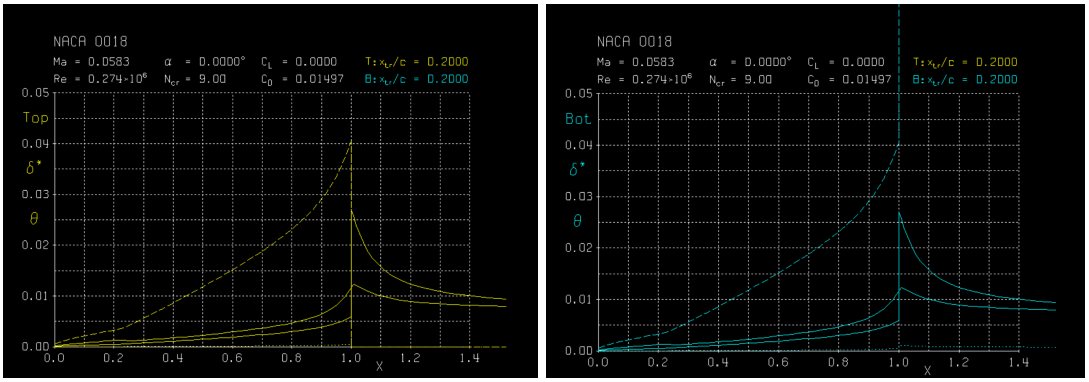

Figure 5: Displacement and Momentum thickness over the top (left) and the bottom (right) side of the airfoil obtained from X-Foil

Unfortunately, the X-foil program does not calculate the boundary layer thickness. Hence, the estimation of the boundary layer thickness is feasible by the usage of the Lee model approximation, which relates the boundary layer and displacement thickness and is given in Equation 3:

$$\delta = 8\delta^* \tag{3}$$

Where δ is the boundary layer thickness and δ^* is the boundary layer displacement thickness. Thus, the calculation of boundary layer thickness is now simplified and it is demonstrated in :

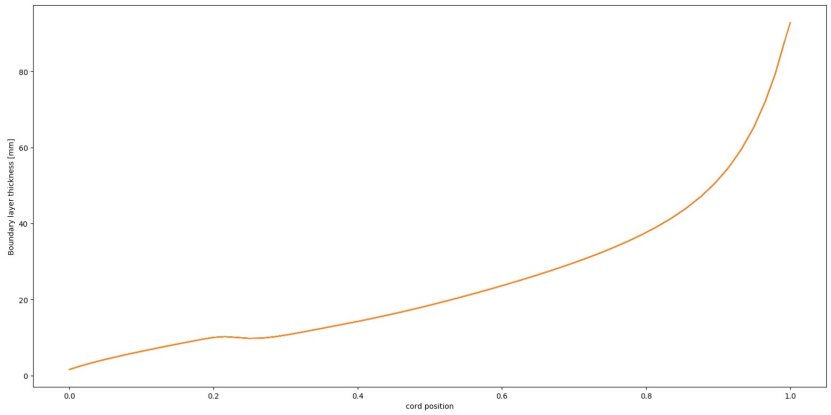

Figure 6: Boundary layer thickness over the airfoil

Finally, as observed in Figure 6, the distribution of the boundary layer thickness on the upper and the lower side of the airfoil is identical, as expected. The boundary layer widens as the flow approaches the trailing edge as the flow is energized by the turbulent mechanism.

1.2 Lee model

1.2.1 Empirical model selection

$$\frac{\Phi(\omega)U_e}{\tau_w^2\delta^*} = \frac{\max\left(a, (0.25\beta_c - 0.52)\, a\right)\left(\omega\delta^*/U_e\right)^2}{\left[4.76\left(\omega\delta^*/U_e\right)^{0.75} + d^*\right]^e + \left[8.8R_T^{-0.57}\left(\omega\delta^*/U_e\right)\right]^{h^*}} \tag{4}$$

$$a = \left[2.82\Delta^2\left(6.13\Delta^{-0.75} + d\right)^e\right] * \left[4.2(\Pi/\delta) + 1\right] \tag{5}$$

$$d = 4.76(1.4/\Delta)^{0.75}[0.375e - 1] \tag{6}$$

$$e = 3.7 + 1.5\beta_c \tag{7}$$

Equation 4 with coefficients Equation 5, Equation 6 and Equation 7 are used to compute the wall-pressure spectrum for the given airfoil with turbulent boundary layer [5]. From the four available papers, only Lee [5] and Kamruzzaman [3] are usable for an airfoil subjected to turbulent flow; Goody [2] is only validated for zero pressure gradient flows and Casalino [1] underestimates noise levels for lower velocities. Lee is preferred over Kamruzzaman due to more accurate noise predictions. The far-field acoustic pressure is then computed by inserting Equation 4 into the given Amiet's model.

1.2.2 model results

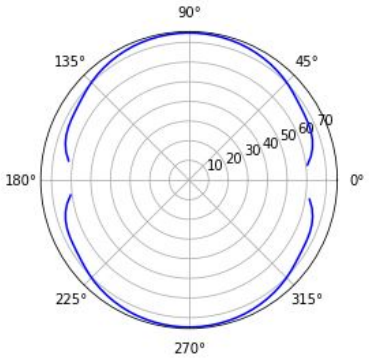

Figure 7: OSPL around trailing edge

Figure 7 shows the total OSPL for frequencies summed up from 1 up to 240000 Hz with a Welch distribution; it is the same frequency domain as used in the numerical model. For the angles, 160 microphones are used spread out over the domain from 0 to 2π radians. Note that the noise output is zero around 0 deg and 180 deg and has a peak magnitude of roughly 70 dB. Shape wise the spectrum is a double circle with zero at the center which is expected for a solid boundary with low free stream velocity ($M_0 c/\lambda << 1$). This shape is also similar to Figure 8 however, the order magnitude is off; an explanation is frequency spectrum input is different for both models.

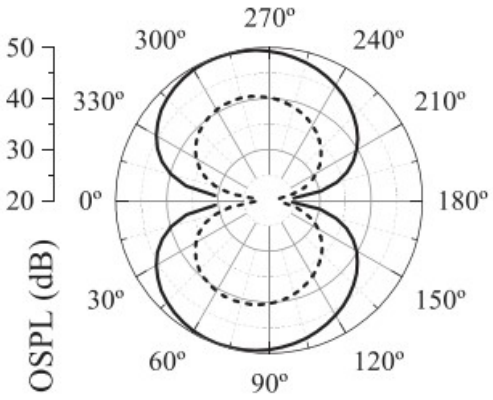

Figure 8: OSPL for $\alpha = 0$ deg and v=0 m/s [6]

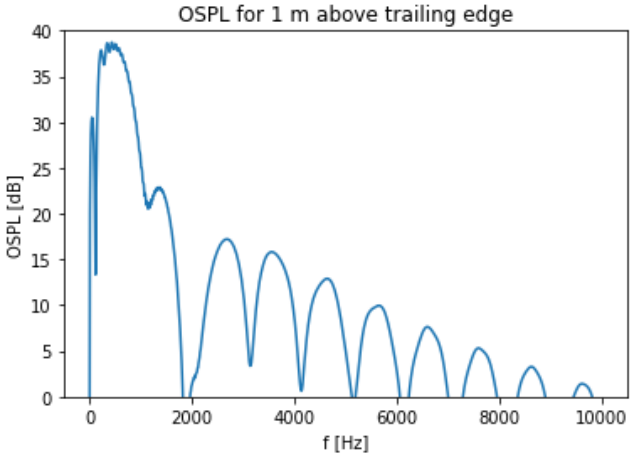

Figure 9: OSPL for frequency range at single point

Another interesting observation is that $\frac{T}{\delta*} = 0.018\frac{0.2}{0.0116} = 0.31$ meaning the trailing edge is considered thick and rounded thus, vortex shredding linked to tonal noise is expected. Figure 9 confirms this observation.

2 High Fidelity Model model

2.1 PowerACOUSTICS Implementation

In order to obtain the far field analysis, the mesh model as well as flow parameters where inputted to PowerACOUSTICS. The circular array consisted of a locus of microphones centered around the trailing edge center. With a radius of one meter, 160 microphones are equally spaced which would enough to be able to give a detailed reproduction of the noise directivity pattern. This data was later processed in Python to obtain Figure 13.

2.2 PowerVIZ Implementation

To obtain the boundary parameters of the high fidelity model PowerVIZ was utilized. To obtain the pressure coefficient the following equation was used:

$$C_p = \frac{p - p_\infty}{\frac{1}{2}\rho_\infty V_\infty^2} \tag{8}$$

Where p is the static pressure, and p_∞ is the static pressure of the free-stream, ρ_∞ is the free stream density, and V_∞ is the free stream velocity . The output from PowerVIZ is obtained in Figure 10

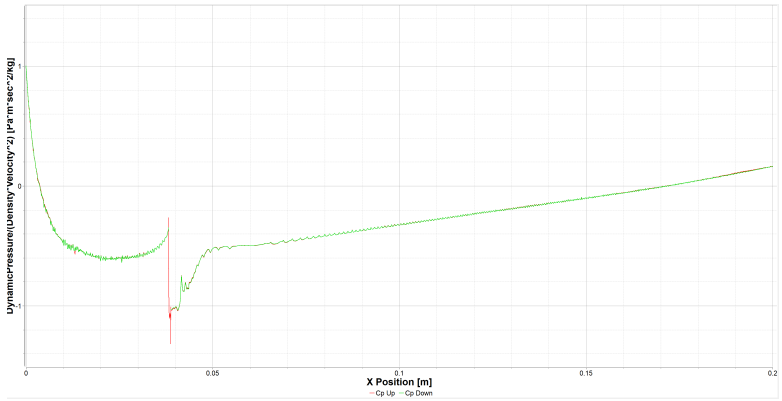

Figure 10: Pressure coefficient of airfoil obtained from PowerVIZ

One can observe the discontuity caused by the trip wire with the sudden drop in pressure as the air is forced from a laminar to a turbulent flow.

To find the shear stress at the wall the following equation was employed:

$$C_f = \frac{\tau_w}{\frac{1}{2}\rho v^2} \tag{9}$$

Where C_f is the skin friction coefficient, τ_w is the skin shear stress and $\frac{1}{2}\rho v^2$ is the dynamic pressure of the unperturbed free stream. From that the following values are acquired Figure 11

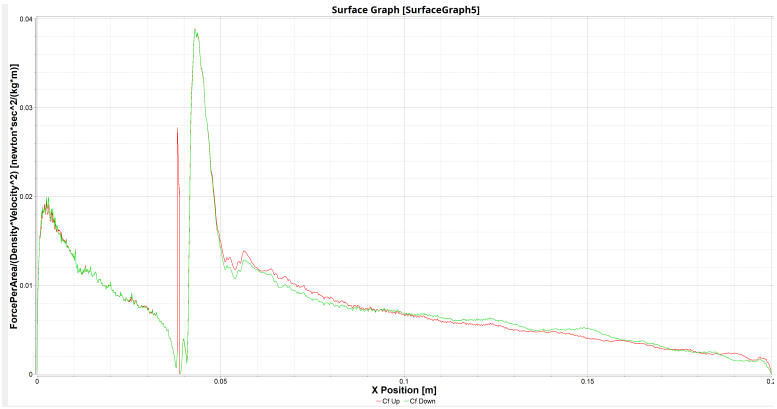

Figure 11: Skin friction coefficient of airfoil obtained from PowerVIZ

In order to obtain the boundary layer parameters, PowerVIZ was furthermore employed, by placing a probe just before the trailing edge it was possible to obtain the velocity profile perpendicular to the trailing edge and thus obtain the boundary layer width and profile velocity in Figure 12.

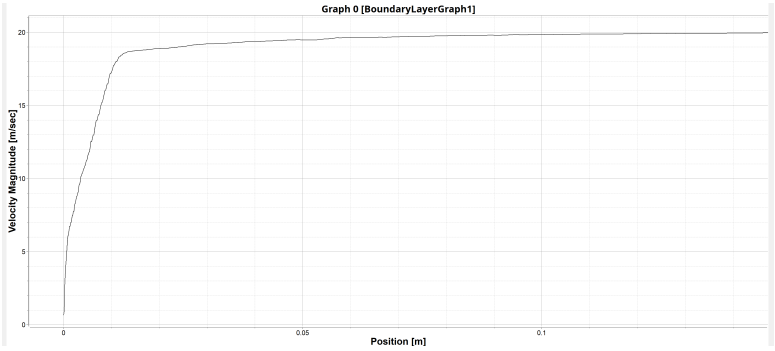

Figure 12: Boundary layer velocity profile obtained from PowerVIZ

2.3 Noise Emission

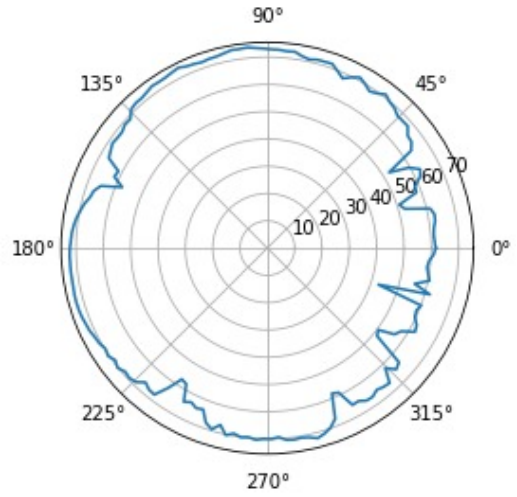

Figure 13: OSPL non-permeable numerical model

Figure 13 shows the noise spectrum for the numerical model. It can be observed from Figure 14 that the spectrum consists of broadband noise.

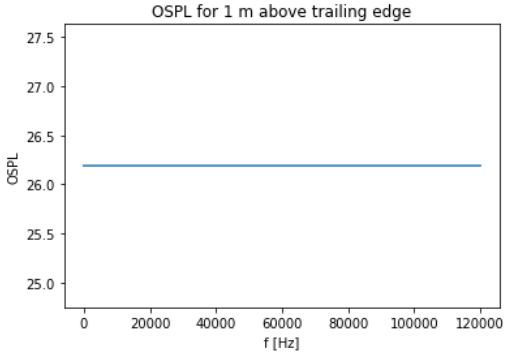

Figure 14: OSPL for sampled frequency domain

3 Comparison

3.1 Flow conditions

The comparison of flow conditions between PowerViz and X-Foil is executed. The main differences between the numerical and analytical models are demonstrated in the following paragraphs:

3.1.1 Comparison of pressure

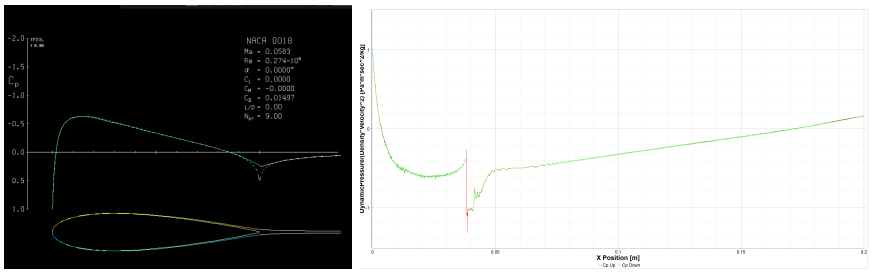

Figure 15: Comparison of pressure coefficient from X-Foil (left) and PowerVIZ (right)

In Figure 15, one observes similar values presented in both X-Foil and the high fidelity model with similar minimas. However a stark contrast at 20% of the chord is visible due to the presence of the trip wire for the PowerVIZ model. Whereas X-Foil can force transition without imposing a pressure coefficient discontinuity, PowerVIZ's physical trip on its geometry means that it has the discontinuity. After the trip the values continue with the same characteristics albeit the slight deviance due to the discontinuity.

3.1.2 Comparison of Skin friction Properties

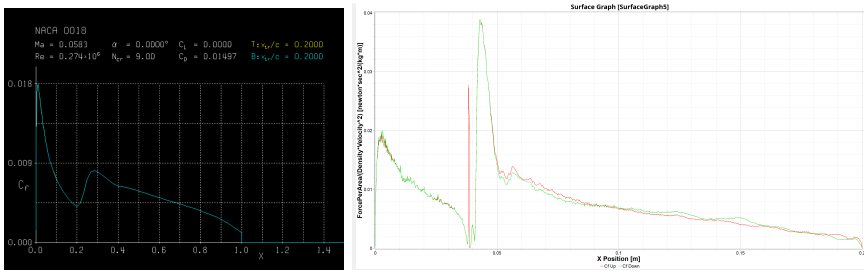

Figure 16: Comparison of skin friction coefficient from X-Foil (left) and PowerVIZ (right)

Once again similar properties from the High fidelity model and X-Foil are present in Figure 16. However, compared to the pressure coefficient graphs, some more differences are evident. Whereas in X-Foil the maximum skin friction is on the leading edge for X-Foil, for PowerVIZ this occurs at the location of the trip. Once again the most probable argumentation for this phenomena is due to the physical nature of the trip for the high fidelity model whereas in X-Foil the turbulence is numerically induced. In fact, the leading edge of X-Foil and PowerVIZ are almost identical in skin friction drag and after the trip both models present similar dissipation modes however the effects of the tripwire mean that the PowerVIZ model experiences a larger skin friction drag post transition.

3.1.3 Comparison of boundary layer properties

For the comparison of the boundary layer properties of the two methods, we are going to evaluate the properties at the trailing edge. First of all, the direct calculation of boundary layer thickness is impossible in PowerViz. The boundary layer thickness δ is calculated by the usage of boundary layer velocity Figure 12 and the following approximation:

$$V_e = 0.99 V_\infty \tag{10}$$

where V_e is the boundary layer velocity and V_∞ the free-stream velocity. This implies that the boundary layer thickness is the distance normal to the trailing edge where Equation 10 is true. Inserting the values we get from PowerViz for the edge velocity in the Equation 10, we can easily derive that the boundary layer thickness is equal:

$$\delta = 0.092472 \quad [\text{m}] \tag{11}$$

To continue with, displacement thickness δ^* is computed by the Lee's model approximation Equation 3 and it shown in the following Equation 12:

$$\delta^* = 0.011559 \quad [\text{m}] \tag{12}$$

The momentum thickness θ can be computed by realising that the turbulence transition was induced in a flow state that would have laminar under normal circumstances [4]. As such the shape factor which gives the boundary layer momentum thickness was taken as the average of their turbulent and laminar values respectively and with that, the following values for the boundary layer momentum thickness where calculated. Equation 13:

$$\theta = 0.006083 \quad [\text{m}] \tag{13}$$

Extracting the corresponding values from the X-Foil we can summarize the results in Table 2:

Table 2: Boundary layer parameters comparison

	δ, [m]	δ^*, [m]	θ, [m]
PowerViz	0.092472	0.011559	0.006083
X-Foil	0.092872	0.011609	0.005869
Deviation	0.43%	0.43%	%3.51

The boundary properties comparison at the trailing edge has shown a high agreement between the two methods. Dissimilar with the previous comparisons, which conduct over the entire airfoil surface, in this case, the results have shown convergence of boundary layer parameters at the trailing edge with a maximum deviation of 3.51%. Hence, these models seem to give similar results for the boundary layer at the trailing edge.

3.2 Noise Emission Comparison

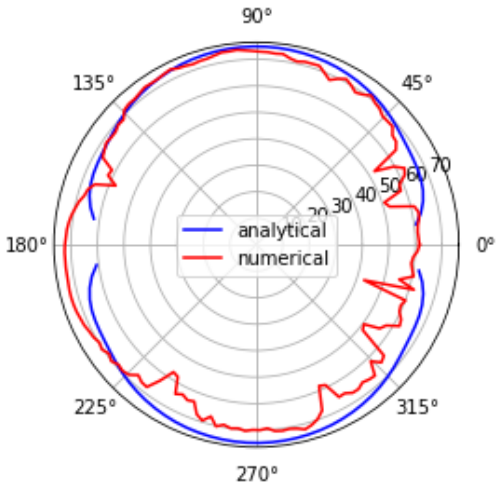

Figure 17: OSPL comparison between numerical and analytical model

Figure 17 shows both models (non-permeable for numerical) plotted in the same figure. The order of magnitude is the same for both models and spectrum has a similar shape at the top and bottom. At the sides the analytical model predicts zero values while the numerical model adheres the airfoil contour. A potential cause for this difference is that the noise output itself varies from the two models; Figure 9 is tonal while Figure 17 is broadband. Overall however, it is proven that the numerical simulation is validated for the given test case due to correctly captured magnitudes.

3.3 Bonus Question Permeable Surface

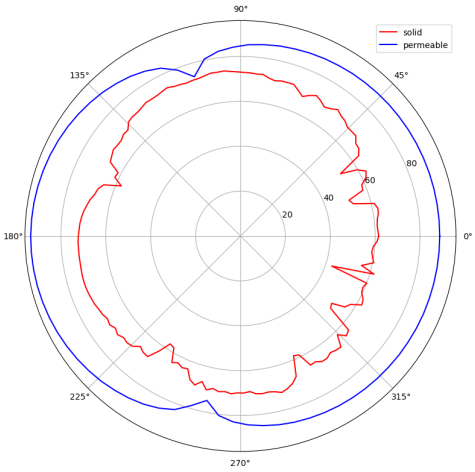

Figure 18: OSPL comparison between solid and permeable models

3.4 Bonus Question other group comparison

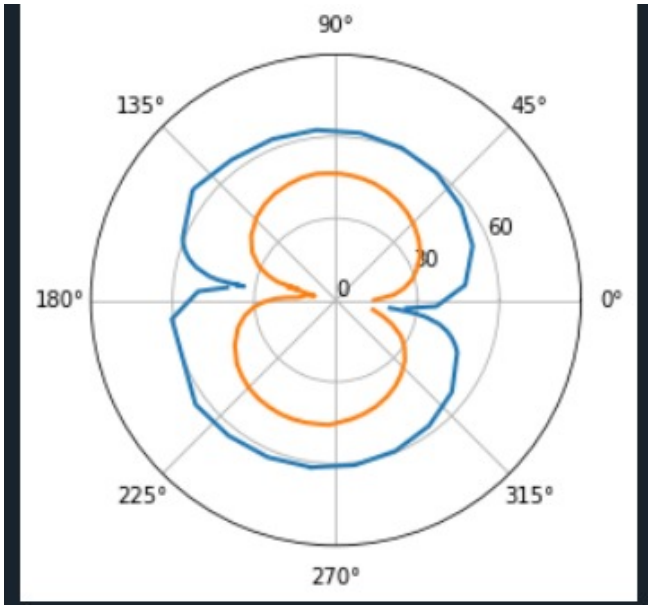

Figure 19: OSPL for $\alpha = 7.8°$ and V=20 m/s

Figure 19 shows the OSPL from another group for a Goody model and solid numerical simulation at $\alpha = 7.8°$ and V=20 m/s. The double circle shape is similar to the results from the analytical $\alpha = 0°$ simulation. The numerical solution is in a similar order of magnitude as both $\alpha = 0°$; slightly lower magnitude. The $\alpha = 7.8°$ analytical model however, under predicts the magnitudes. This can be explained by the fact that the Goody model is only validated for zero pressure gradient flat plate flows and proven inaccurate for airfoils [5].

References

Casalino, D., & Barbarino, M. (2010). A stochastic method for airfoil self-noise computation in frequency-domain. *AIAA Journal*, *16*.

Goody, M. (2004). Empirical spectral model of surface pressure fluctuations. *AIAA Journal*, *42*(9).

Kamruzzaman, M., Bekiropoulos, D., Lutz, T., Würz, W., & Krämer, E. (2015). A semi-empirical surface pressure spectrum model for airfoil trailing-edge noise prediction. *International journal of aeroacoustics*, *14*(5,6).

Kotsonis, M., Michelis, T., & van Oudheusden, D. B. (2021). Viscous flows module 1a: Fundamentals of boundary layers 1..

Lee, S. (2018). Empirical wall-pressure spectral modeling for zero and adverse pressure gradient flows. *AIAA Journal*, *56*(5).

Teruna, C., Avallone, F., & Ragni, D. (n.d.). On the noise reduction of a porous trailing edge applied to an airfoil at lifting condition.